HHS Public Access

Author manuscript

Med Biol Eng Comput. Author manuscript; available in PMC 2017 May 01.

Published in final edited form as:

Med Biol Eng Comput. 2016 May ; 54(5): 799–809. doi:10.1007/s11517-015-1371-y.

Biomechanical Evaluation of the Pathophysiologic Developmental Mechanisms of Mitral Valve Prolapse: Effect of Valvular Morphologic Alteration

Ahnryul Choi, **David D. McPherson**, and **Hyunggun Kim**[§]

Division of Cardiovascular Medicine, Department of Internal Medicine, The University of Texas Health Science Center at Houston, Houston, Texas, USA

Abstract

Mitral valve prolapse (MVP) refers to an excessive billowing of the mitral valve (MV) leaflets across the mitral annular plane into the left atrium during the systolic portion of the cardiac cycle. The underlying mechanisms for the development of MVP and mitral regurgitation (MR) in association with MV tissue remodeling is still unclear. We performed computational MV simulations to investigate the pathophysiologic developmental mechanisms of MVP. A parametric MV geometry model was utilized for this study. Posterior leaflet enlargement and posterior chordal elongation models were created by adjusting the geometry of the posterior leaflet and chordae, respectively. Dynamic finite element simulations of MV function were performed over the complete cardiac cycle. Computational simulations demonstrated that enlarging posterior leaflet area increased large stress concentration in the posterior leaflets and chordae, and posterior chordal elongation decreased leaflet coaptation. When MVP was accompanied by both posterior leaflet enlargement and chordal elongation simultaneously, the posterior leaflet was exposed to extremely large prolapse with a substantial lack of leaflet coaptation. These data indicate that MVP development is closely related to tissue alterations of the leaflets and chordae. This biomechanical evaluation strategy can help us better understand the pathophysiologic developmental mechanisms of MVP.

Keywords

Mitral valve; Mitral valve prolapse; Chordal elongation; Leaflet budging; Finite element; Simulation

1. Introduction

Mitral valve prolapse (MVP) refers to an excessive billowing of the mitral valve (MV) leaflets across the mitral annular plane into the left atrium during the systolic portion of the cardiac cycle [40]. Recent studies report that the prevalence of MVP is close to 2-3% of the

[§]Correspondence: Division of Cardiovascular Medicine, Department of Internal Medicine, The University of Texas Health Science Center at Houston, 6431 Fannin St, MSB 1.246, Houston, Texas 77030, USA, Phone: +1-713-486-2342, Fax: +1-713-500-6556, hyunggun.kim@uth.tmc.edu.

Conflict of Interest

The authors declare that they have no conflict of interest.

total population [39]. Worsening of MVP is closely related to the occurrence of severe mitral regurgitation (MR), which can lead to arrhythmias and congestive heart failure [11]. The most common pathology of MVP involves with the posterior middle scallop (P2), which then extends to the P1 and P3 scallops [16].

Physical examination and echocardiography are the standard methods for diagnosis of MVP. When physicians hear a dynamic mid-to-late systolic click often associated with a high-pitched late systolic murmur using a stethoscope, it is a common procedure to call for additional echocardiographic examination for the patient [3, 16]. Echocardiography provides quantitative information pertaining to abnormal leaflet displacement beyond the annular plane, which is a crucial factor to diagnose MVP. Although morphologic alteration of MV geometry and transvalvular flow characteristics across the MV can be evaluated in real time using echocardiography, it is difficult to study the pathophysiologic developmental mechanisms of MVP using echocardiographic image data alone. Computational evaluation approaches can provide valuable additive information to better understand the biomechanical and pathophysiologic developmental mechanisms of MVP [9, 22, 36, 38, 42, 44].

There are a variety of biological, biochemical, and biomechanical factors involved in the development of MVP. Morphologic alteration of the MV apparatus leads to enhancement of localized stress concentration and tissue degeneration [2]. Myxomatous tissue degeneration with proliferation of the spongiosa layer of the mitral leaflets is a principal factor in MVP [15, 32]. As MVP develops, biomechanical conditions of the prolapsed leaflet area are changed, adverse tissue alteration occurs, and this tissue remodeling yields worsening of prolapse [14]. Myxomatous MV tissue generally exhibits lower stiffness values with lower failure stresses compared to normal MV tissue [4, 5]. Increased chordal length and altered chordal stiffness are closely related to the extent and severity of leaflet enlargement and initiation of MVP [17, 18]. When MVP further progresses to severe MVP, not only local leaflet coaptation deteriorates leading to considerable MR [20], but chordal rupture is often found with severe MVP [1].

In this study, we performed virtual MV simulations to investigate the pathophysiologic developmental mechanisms of MVP. Effects of leaflet enlargement and chordal elongation on MV dynamics were evaluated. The hypothesis was that the enlarging leaflet area affects the severity of MVP leading to increase chordal stresses, and that the elongated chordae tendineae deteriorates into worsening of the MR.

2. Methods

2.1. Virtual MV modeling

A parametric normal MV geometry model at end diastole (Fig. 1A) was designed for this MVP mechanistic study using similar techniques as described in previous studies [38, 42, 43]. Based on anatomical literatures [23, 41], the representative structural dimensions of the saddle-shaped annulus, the anterior leaflet, the tri-scalloped posterior leaflet, the marginal and strut chordae tendineae, and the papillary muscles were implemented into this computational MV model. The whole MV model was designed to be symmetric with respect to the plane perpendicular to the orifice and aligned to the A-P line of the annulus. The

saddle-shaped annulus was created utilizing the key landmark information (A, P, Al and Pm) and a cubic spline interpolation method (MATLAB, The Mathworks Inc, Natick, MA, USA). The free edge of the leaflets was generated using a linear combination of sinusoidal functions, and multiple lines connecting the annulus and the free edge of the leaflets were modeled [43]. The non-uniform rational B-spline (NURBS) surface modeling method was utilized to create a three-dimensional surface model of the mitral leaflets and annulus. This model was imported into ABAQUS software (SIMULIA, Providence, RI, USA) and meshed using triangular shell elements (S3R element type). The papillary muscle tips were located 28 mm from the plane of annulus with a distance of 18 mm between the two papillary muscle tips [41]. A total of 24 marginal chordae tendineae were modeled as 3D line elements (T3D2 element type) connecting the free edge of the leaflets and the papillary muscles. The two strut chordae tendineae were modeled by connecting the top portion of the rough zone of the anterior leaflet [23] and the papillary muscles. The chordal insertion was distributed around the papillary muscles.

2.2. Pathologic MV models with leaflet enlargement and chordal elongation

Fig. 1B depicts the computational models of pathologic MVs with mild and severe P2 leaflet enlargement. Three-dimensional transesophageal echocardiography provides detailed morphologic information pertaining to leaflet billowing and chordal lengths for diagnosing posterior MVP [16, 40]. Clinical guidelines indicate that posterior leaflet billowing greater than 2 mm during systole should be considered severe MVP. The pathologic MV models were created to attain this level of leaflet billowing at peak systole.

P2 leaflet enlargement was modeled such that the maximal protruding distance in the mid-P2 region was equivalent to a quarter or a half of the P2 annulus-to-leaflet free edge distance (d) for the mild and severe P2 leaflet enlargement models, respectively. The posterior chordal elongation models were created by modeling longer posterior marginal chordae than the normal MV. The P2 chordae were elongated by 25% and 50% to model the mild and severe posterior chordal elongation models, respectively. Other posterior chordae were proportionally elongated towards the commissural (Al and Pm) free edge of the leaflets.

2.3. Finite element simulation of MV function

A Fung-type elastic constitutive model was implemented to incorporate the anisotropic hyperelastic material characteristics of the MV leaflets [38]. The Cauchy stress (σ) and the Green-Lagrange strain (*E*) can be described as

$$\sigma=\frac{1}{J}\mathbf{F}\frac{\partial W}{\partial E}\mathbf{F}^{T} \quad (1)$$

where J is the determinant of the deformation gradient (**F**). The strain energy function W is defined using four parameters (c, A_1, A_2 and A_3) as

$$W=\frac{c}{2}\left[e^{Q}-1\right], \quad Q=A_1E_{11}^2+A_2E_{22}^2+2A_3E_{11}E_{22} \quad (2)$$

The stress-strain relationship of a nearly incompressible hyperelastic material (J = det **F** = 1) is given by

$$\sigma_c = (2E_{11}+1)\, c\, exp\,(Q)\,(A_1E_{11}+A_3E_{22}) \quad (3)$$

$$\sigma_r = (2E_{22}+1)\, c\, exp\,(Q)\,(A_3E_{11}+A_2E_{22}) \quad (4)$$

The principal material directions were defined along the circumferential (σ_c) and radial (σ_r) directions. Experimentally-determined material parameters obtained from the biaxial mechanical test data of the anterior and posterior leaflet tissue from a previous study [29] were incorporated into the Fung-type elastic model. The Fung-type elastic material model was then implemented into ABAQUS/Explicit (SIMULIA, Providence, RI). Leaflet thicknesses of the anterior and posterior leaflets were set to be 0.69 mm and 0.51 mm, respectively [28].

The Ogden model was employed to define the nonlinear hyperelastic material behavior of the chordae tendineae. Cross-sectional areas were set 0.29 mm^2 for the anterior marginal chordae, 0.27 mm^2 for the posterior marginal chordae, and 0.61 mm^2 for the two strut chordae [34].

The density and Poisson's ratio of the leaflets and chordae tendineae were set 1,100 kg/m^3 and 0.48, respectively [38, 43]. A time-varying physiologic transvalvular pressure gradient was applied on the ventricular and atrial sides of the leaflet surface in the normal direction across the complete cardiac cycle. The maximum systolic transvalvular pressure value was 16.8 kPa (126 mmHg) [31]. Both leaflet-to-leaflet and leaflet-to-chordae contact interactions were considered for leaflet coaptation, and the friction coefficient was assumed to be 0.05 [42]. Further details of dynamic finite element simulation of MV function are described in our previous studies.

2.4. Study design and data analysis

Leaflet stress distributions and maximum chordal stress values at peak systole were compared between the normal MV and the MVs with mild P2 leaflet enlargement or severe P2 leaflet enlargement [17, 18]. Effects of chordal elongation on leaflet stress distribution and leaflet coaptation at peak systole were compared between the MV models having normal pathophysiology, mild posterior chordal elongation, and severe posterior chordal elongation. Combined effects of severe P2 leaflet enlargement and posterior chordal elongation were investigated in terms of geometric and functional characteristics of MV dynamics at peak systole. Leaflet morphology, coaptation length, and posterior billowing height in the anteroposterior cross-sectional planes were compared between the MV models having normal pathophysiology, severe P2 leaflet enlargement, severe posterior chordal elongation, and a combination of these two abnormalities. Coaptation length was measured in the coapted leaflet region in the anteroposterior planes. Posterior billowing height was determined by measuring the height from the A-P line connecting the anterior and posterior mitral annular positions to the maximum protruding point of the posterior leaflet into the left atrium.

3. Results

3.1. Dynamic FE simulation of MV function

Fig. 2 demonstrates the morphologic characteristics of the normal MV at five representative time points over the cardiac cycle. Dynamic FE simulation provided detailed structural information of each component of the MV apparatus. The same dynamic FE methods were utilized for all simulations in this study. This indicates that the parametric MV models have been successfully implemented into our dynamic FE protocol to simulate MV function across the cardiac cycle.

3.2. Effects of P2 leaflet enlargement

Posterior leaflet enlargement clearly affected stress distributions across the mitral leaflets and annulus at peak systole (Fig. 3). The maximal stress values increased in proportion to the severity of P2 leaflet enlargement (normal MV = 0.60 MPa, mild P2 leaflet enlargement = 0.64 MPa, and severe P2 leaflet enlargement = 0.99 MPa). Excessive stress concentration along the radial direction was found in the posterior leaflet when posterior leaflet enlargement occurred. In all three MVs, a similar pattern of stress distribution was observed in the anterior leaflet displaying large stresses near the mitral annulus-aorta junction region regardless of the presence of posterior leaflet enlargement.

The maximal chordal stress values were found in the P2 region where leaflet enlargement occurred (Fig. 4). Mild and severe P2 leaflet enlargement increased the maximal P2 chordal stress by 12% and 31% compared to the normal MV, respectively. The average maximal chordal stress values in the P1 (593 kPa vs. 605 kPa vs. 598 kPa) and P3 (585 kPa vs. 595 kPa vs. 600 kPa) regions were comparable between the normal MV and the MVs with mild and severe P2 leaflet enlargement.

3.3. Effects of posterior chordal elongation

Leaflet coaptation at peak systole in the normal MV and the MVs with posterior chordal elongation is demonstrated in Fig. 5. Full leaflet coaptation was clearly observed in the normal MV. With mild or severe posterior chordal elongation, substantial posterior leaflet prolapse occurred. A distinct lack of leaflet coaptation was found in the P2 scallop.

Fig. 6 demonstrates stress distributions across the mitral leaflets and annulus at peak systole in the normal MV and the MVs with posterior chordal elongation. There was little difference in magnitudes of the maximal stress values between the three MV models. In the presence of severe posterior chordal elongation, stress concentration was found in the middle belly region of the anterior leaflet presumably due to the lack of coaptation in this region following posterior leaflet prolapse.

3.4. Combined effects of posterior leaflet enlargement and chordal elongation

Leaflet morphologies at peak systole with severe P2 leaflet enlargement, severe posterior chordal elongation, and a combination of these two abnormalities were compared to normal (Fig. 7). In order to better demonstrate the degree of leaflet coaptation and the severity of leaflet billowing, the cross-sectional edges of the anterior and posterior leaflets along the

A2-P2 and A3-P3 planes are displayed in blue and red, respectively. Both severe P2 leaflet enlargement and severe posterior chordal elongation resulted in increased posterior leaflet prolapse. In the A3-P3 plane, severe posterior chordal elongation resulted in larger leaflet malcoaptation than severe P2 leaflet enlargement only. With severe P2 leaflet enlargement and severe posterior chordal elongation together, an extremely large prolapse was observed across the entire posterior leaflet, and leaflet coaptation was markedly deteriorated vs. with each anomaly alone.

Coaptation lengths along the A2-P2 and A3-P3 planes in the MVs having normal pathophysiology, severe P2 enlargement, severe posterior chordal elongation, and a combination of these two abnormalities are demonstrated in Fig. 8A. There were clear differences in physiologic abnormalities of MV function between these MV models in terms of coaptation length. In the normal MV, the coaptation lengths in the A2-P2 and A3-P3 planes were 6.2 mm and 3.2 mm, respectively. The MV with severe P2 enlargement demonstrated an increased coaptation length of 9.1 mm in the A2-P2 plane presumably due to the enlarged posterior leaflet surface in the P2 region while retaining a similar to normal coaptation length in the A3-P3 plane. In contrast, the MV with severe posterior chordal elongation revealed markedly reduced coaptation lengths in both the A2-P2 (1.3 mm) and A3-P3 (no coaptation) planes. The MV with a combination of severe P2 enlargement and severe posterior chordal elongation exhibited no leaflet coaptation in either the A2-P2 or the A3-P3 plane.

The MV models with any type of pathologic abnormality demonstrated increased posterior billowing heights compared to the normal MV (Fig. 8B). The posterior billowing height of the normal MV were 0.59 mm and 0.29 mm in the A2-P2 and A3-P3 planes, respectively. Severe P2 leaflet enlargement resulted in an increased posterior billowing height (3.0 mm), and the MV with severe posterior chordal elongation showed a larger billowing height (4.0 mm) in the A2-P2 plane. The MV with a combination of severe P2 enlargement and severe posterior chordal elongation revealed a 13 times larger billowing height (7.8 mm) in the A2-P2 plane compared to normal. A similar pattern of billowing height increase was found in the A3-P3 planes.

Discussion

MVP due to myxomatous leaflet degeneration is the most common etiology of MR requiring MV repair when the MR becomes severe [14]. Myxomatous degeneration induces tissue alteration of the MV apparatus, often leading to physiologic and functional deterioration of the leaflets and chordae. Although these alterations of tissue characteristics of the leaflets and chordae tendineae have been actively studied [4, 5, 12, 30], the underlying biomechanical mechanisms for the development of MVP and MR in association with valvular morphologic alteration are still unclear. In this study, we investigated the effects of enlarged leaflet tissue and elongated chordae on leaflet stress, chordal stress, and leaflet coaptation from a biomechanical perspective.

Clinical criteria for diagnosis of MVP involve several morphologic characteristics of the MV apparatus [3, 10, 14, 33]. These include the extents of leaflet area enlargement, leaflet

billowing toward the left atrium, interchordal leaflet arching, and annular dilation. Computational MV simulations can provide valuable information pertaining to the effect of each morphologic alteration in MVP development. We found large stresses over the posterior leaflet when P2 leaflet enlargement occurred (Fig. 3). Enlarged leaflet led to increased surface area when exposed to transvalvular pressures. This resulted in increased stresses in the chordae connected to the leaflet margins (Fig. 4). Increased chordal stress can induce elongation of the chordae tendineae in the long term [17, 18]. Computational simulations revealed a decrease of leaflet coaptation when the posterior chordae were elongated (Fig. 5). When the MV was accompanied by both leaflet enlargement and chordal elongation simultaneously, the leaflets were exposed to extremely large prolapse with a substantial lack of leaflet coaptation (Figs. 7 and 8). These data indicate that MVP development is closely related to morphologic alterations of the mitral leaflets and chordae, and computational evaluation of biomechanical characteristics of MV function can provide quantitative information in terms of the pathophysiologic developmental mechanisms of MVP.

We utilized previously published material properties of the MV apparatus components in the computational simulations due to the limited availability of the material properties of human MV tissue [38]. Both mechanical properties and physical dimensions (e.g., tissue thickness) of myxomatous MV leaflets and chordae tendineae are different from healthy MV tissue [4, 5, 13, 35]. Implementation of actual tissue properties of myxomatous MVs would affect the results of the FE simulations. The primary focus of this study is to evaluate the effect of valvular morphologic alteration (i.e., leaflet enlargement and/or choral elongation) on biomechanical and physiologic characteristics of MV function. Therefore, we implemented the same tissue properties into both normal and pathologic MV models, and compared the biomechanical and physiologic characteristics of MV function when leaflet enlargement, chordal elongation, or a combination of these two abnormalities occurs. Our computational MV evaluation protocol can be easily implemented with any types of tissue material model. More realistic material characteristics of (both normal and pathologic) human MV tissue will be incorporated as soon as experimental data or validated material properties [21] are available.

There are some limitations and simplifications that need to be clearly specified in this study. We employed a simplified parametric MV model. The entire MV structure was assumed symmetric to determine the subsequent biomechanical and physiologic effects following each valvular morphologic anomaly. This indicates that any asymmetry of the native MV geometric characteristics is neglected [7]. Although others and our group have demonstrated rigorous validation studies in parametric MV modeling [42, 43] and FE simulations of MV function [37, 38], sensitivity analysis [26] has not been performed in this study. With these parametric MV models, computational simulations of MV function following posterior leaflet enlargement and/or chordal elongation clearly demonstrated the effects of the valvular morphologic alterations. The FE-predicted leaflet deformation in the parametric normal MV in this study may not represent a purely typical “normal” MV. We found sufficient clinical and anatomical literatures to define the marginal and strut chordae, but due to limited availability of information clearly describing the structure and distribution over the MV leaflets [6, 24], the basal chordae were not included in the MV models in this study.

This would result in over-protruding of the leaflets towards the left atrium at peak systole. Lastly, the hemodynamic effect of blood flow was not considered in this study. We have recently published clinical case studies to accurately simulate MV dynamics of various pathologic conditions using our dynamic finite element protocol [37, 38]. It is anticipated that incorporation of realistic fluid-induced loading conditions on the valve cusps (e.g., physiologic 3D fluid-structure interaction simulation) will provide more accurate information pertaining to valvular dynamics [8, 19, 25, 27].

What is the utility of better understanding of the pathophysiologic developmental mechanisms of MVP from a biomechanical perspective? Presently our surgical techniques for MV repair rely on the surgeon's ability to accurately quantify the amount of prolapse that requires leaflet resection. Chordal repair generally do not occur when leaflet resection is being performed. If a more quantitative pathophysiologic measure of leaflet and chordal deformity can be obtained, then patient-specific MV repairs can be performed with better and more durable outcomes. This will occur when pathophysiologic effects of MVP can be quantitated.

Conclusions

We have successfully investigated the effects of leaflet enlargement and chordal elongation on MVP development using computational evaluation techniques. Enlarging leaflet area increased large stress concentration in the leaflets and chordae, and chordal elongation decreased leaflet coaptation. This biomechanical evaluation strategy can help us better understand the pathophysiologic developmental mechanisms of MVP.

Supplementary Material

Refer to Web version on PubMed Central for supplementary material.

Acknowledgements

This work was supported in part by the National Institutes of Health (R01 HL109597).

Authors biography

Ahnryul Choi is a postdoctoral fellow in the Department of Internal Medicine at The University of Texas Health Science Center at Houston. He received his Ph.D. degree in Biomedical Engineering from Sungkyunkwan University. His research interests include the development of computational modeling and simulation techniques for heart valve evaluation.

David D. McPherson is the Chair and a Professor of the Department of Internal Medicine at The University of Texas Health Science Center at Houston. He received his M.D. degree in Medicine from The University of Alberta. His research interests include the development of new ultrasound techniques for advanced imaging and therapeutic delivery, the development of three-dimensional techniques for cardiac and vascular reconstruction, and the evaluation of valvular heart diseases.

Hyunggun Kim is an Associate Professor of the Department of Internal Medicine at The University of Texas Health Science Center at Houston. He received his Ph.D. degree in Biomedical Engineering from The University of Iowa. His research interests include the development of advanced computational techniques for patient-specific heart valve evaluation and the development of molecular ultrasound imaging techniques.

References

1. Agozzino L, Falco A, de Vivo F, de Vincentiis C, de Luca L, Esposito S, Cotrufo M. Surgical pathology of the mitral valve: gross and histological study of 1288 surgically excised valves. Int J Cardiol. 1992; 37:79–89. [PubMed: 1428293]
2. Amini R, Eckert CE, Koomalsingh K, McGarvey J, Minakawa M, Gorman JH, Gorman RC, Sacks MS. On the in vivo deformation of the mitral valve anterior leaflet: effects of annular geometry and referential configuration. Ann Biomed Eng. 2012; 40:1455–1467. Doi 10.1007/s10439-012-0524-5. [PubMed: 22327292]
3. Attenhofer Jost CH, Turina J, Mayer K, Seifert B, Amann FW, Buechi M, Facchini M, Brunner-La Rocca HP, Jenni R. Echocardiography in the evaluation of systolic murmurs of unknown cause. Am J Med. 2000; 108:614–620. [PubMed: 10856408]
4. Barber JE, Kasper FK, Ratliff NB, Cosgrove DM, Griffin BP, Vesely I. Mechanical properties of myxomatous mitral valves. J Thorac Cardiovasc Surg. 2001; 122:955–962. Doi 10.1067/mtc.2001.117621. [PubMed: 11689801]
5. Barber JE, Ratliff NB, Cosgrove DM 3rd, Griffin BP, Vesely I. Myxomatous mitral valve chordae. I: Mechanical properties. J Heart Valve Dis. 2001; 10:320–324. [PubMed: 11380094]
6. Castillo JG, Solis J, Gonzalez-Pinto A, Adams DH. Surgical echocardiography of the mitral valve. Rev Esp Cardiol. 2011; 64:1169–1181. Doi 10.1016/j.recesp.2011.06.025. [PubMed: 22032935]

7. Dagum P, Timek TA, Green GR, Lai D, Daughters GT, Liang DH, Hayase M, Ingels NB Jr. Miller DC. Coordinate-free analysis of mitral valve dynamics in normal and ischemic hearts. Circulation. 2000; 102:III62–69. [PubMed: 11082364]
8. Dahl SK, Vierendeels J, Degroote J, Annerel S, Hellevik LR, Skallerud B. FSI simulation of asymmetric mitral valve dynamics during diastolic filling. Comput Methods Biomech Biomed Engin. 2012; 15:121–130. Doi 10.1080/10255842.2010.517200. [PubMed: 21086206]
9. Einstein DR, Kunzelman KS, Reinhall PG, Cochran RP, Nicosia MA. Haemodynamic determinants of the mitral valve closure sound: a finite element study. Med Biol Eng Comput. 2004; 42:832–846. [PubMed: 15587476]
10. Foster GP, Isselbacher EM, Rose GA, Torchiana DF, Akins CW, Picard MH. Accurate localization of mitral regurgitant defects using multiplane transesophageal echocardiography. Ann Thorac Surg. 1998; 65:1025–1031. [PubMed: 9564922]
11. Freed LA, Levy D, Levine RA, Larson MG, Evans JC, Fuller DL, Lehman B, Benjamin EJ. Prevalence and clinical outcome of mitral-valve prolapse. N Engl J Med. 1999; 341:1–7. Doi 10.1056/NEJM199907013410101. [PubMed: 10387935]
12. Grande-Allen KJ, Barber JE, Klatka KM, Houghtaling PL, Vesely I, Moravec CS, McCarthy PM. Mitral valve stiffening in end-stage heart failure: evidence of an organic contribution to functional mitral regurgitation. J Thorac Cardiovasc Surg. 2005; 130:783–790. Doi 10.1016/j.jtcvs.2005.04.019. [PubMed: 16153929]
13. Gupta V, Barzilla JE, Mendez JS, Stephens EH, Lee EL, Collard CD, Laucirica R, Weigel PH, Grande-Allen KJ. Abundance and location of proteoglycans and hyaluronan within normal and myxomatous mitral valves. Cardiovasc Pathol. 2009; 18:191–197. Doi 10.1016/j.carpath.2008.05.001. [PubMed: 18621549]
14. Guy TS, Hill AC. Mitral valve prolapse. Annu Rev Med. 2012; 63:277–292. Doi 10.1146/annurev-med-022811-091602. [PubMed: 22248324]
15. Hayek E, Griffin B. Mitral valve prolapse: old beliefs yield to new knowledge. Cleve Clin J Med. 2002; 69:889–896. [PubMed: 12430974]
16. Hayek E, Gring CN, Griffin BP. Mitral valve prolapse. Lancet. 2005; 365:507–518. Doi 10.1016/S0140-6736(05)17869-6. [PubMed: 15705461]
17. Jimenez JH, Soerensen DD, He Z, He S, Yoganathan AP. Effects of a saddle shaped annulus on mitral valve function and chordal force distribution: an in vitro study. Ann Biomed Eng. 2003; 31:1171–1181. [PubMed: 14649491]
18. Jimenez JH, Soerensen DD, He Z, Ritchie J, Yoganathan AP. Mitral valve function and chordal force distribution using a flexible annulus model: an in vitro study. Ann Biomed Eng. 2005; 33:557–566. [PubMed: 15981857]
19. Khalafvand SS, Ng EY, Zhong L, Hung TK. Fluid-dynamics modelling of the human left ventricle with dynamic mesh for normal and myocardial infarction: preliminary study. Comput Biol Med. 2012; 42:863–870. Doi 10.1016/j.compbiomed.2012.06.010. [PubMed: 22795507]
20. Kolibash AJ. Progression of mitral regurgitation in patients with mitral valve prolapse. Herz. 1988; 13:309–317. [PubMed: 3053383]
21. Krishnamurthy G, Ennis DB, Itoh A, Bothe W, Swanson JC, Karlsson M, Kuhl E, Miller DC, Ingels NB Jr. Material properties of the ovine mitral valve anterior leaflet in vivo from inverse finite element analysis. Am J Physiol Heart Circ Physiol. 2008; 295:H1141–H1149. Doi 10.1152/ajpheart.00284.2008. [PubMed: 18621858]
22. Kunzelman KS, Quick DW, Cochran RP. Altered collagen concentration in mitral valve leaflets: biochemical and finite element analysis. Ann Thorac Surg. 1998; 66:S198–205. [PubMed: 9930448]
23. Lam JH, Ranganathan N, Wigle ED, Silver MD. Morphology of the human mitral valve. I. Chordae tendineae: a new classification. Circulation. 1970; 41:449–458. [PubMed: 5415982]
24. Lee AP, Hsiung MC, Salgo IS, Fang F, Xie JM, Zhang YC, Lin QS, Looi JL, Wan S, Wong RH, et al. Quantitative analysis of mitral valve morphology in mitral valve prolapse with real-time 3-dimensional echocardiography: importance of annular saddle shape in the pathogenesis of mitral regurgitation. Circulation. 2013; 127:832–841. Doi 10.1161/CIRCULATIONAHA.112.118083. [PubMed: 23266859]

25. Maleki H, Shahriari S, Durand LG, Labrosse MR, Kadem L. A metric for the stiffness of calcified aortic valves using a combined computational and experimental approach. Med Biol Eng Comput. 2014; 52:1–8. Doi 10.1007/s11517-013-1113-y. [PubMed: 24037347]
26. Mansi T, Voigt I, Georgescu B, Zheng X, Mengue EA, Hackl M, Ionasec RI, Noack T, Seeburger J, Comaniciu D. An integrated framework for finite-element modeling of mitral valve biomechanics from medical images: application to MitralClip intervention planning. Med Image Anal. 2012; 16:1330–1346. Doi 10.1016/j.media.2012.05.009. [PubMed: 22766456]
27. Marom G, Haj-Ali R, Raanani E, Schafers HJ, Rosenfeld M. A fluid-structure interaction model of the aortic valve with coaptation and compliant aortic root. Med Biol Eng Comput. 2012; 50:173–182. Doi 10.1007/s11517-011-0849-5. [PubMed: 22170305]
28. May-Newman K, Yin FC. Biaxial mechanical behavior of excised porcine mitral valve leaflets. Am J Physiol. 1995; 269:H1319–1327. [PubMed: 7485564]
29. May-Newman K, Yin FC. A constitutive law for mitral valve tissue. J Biomech Eng. 1998; 120:38–47. [PubMed: 9675679]
30. Mills WR, Barber JE, Ratliff NB, Cosgrove DM 3rd, Vesely I, Griffin BP. Biomechanical and echocardiographic characterization of flail mitral leaflet due to myxomatous disease: further evidence for early surgical intervention. Am Heart J. 2004; 148:144–150. Doi 10.1016/j.ahj.2004.01.021. [PubMed: 15215804]
31. Mitchell JR, Wang JJ. Expanding application of the Wiggers diagram to teach cardiovascular physiology. Adv Physiol Educ. 2014; 38:170–175. Doi 10.1152/advan.00123.2013. [PubMed: 24913453]
32. Olsen EG, Al-Rufaie HK. The floppy mitral valve. Study on pathogenesis. Br Heart J. 1980; 44:674–683. [PubMed: 7459151]
33. Omran AS, Woo A, David TE, Feindel CM, Rakowski H, Siu SC. Intraoperative transesophageal echocardiography accurately predicts mitral valve anatomy and suitability for repair. J Am Soc Echocardiogr. 2002; 15:950–957. [PubMed: 12221412]
34. Prot V, Skallerud B, Sommer G, Holzapfel GA. On modelling and analysis of healthy and pathological human mitral valves: two case studies. J Mech Behav Biomed Mater. 2010; 3:167–177. Doi 10.1016/j.jmbbm.2009.05.004. [PubMed: 20129416]
35. Rausch MK, Kuhl E. On the mechanics of growing thin biological membranes. J Mech Phys Solids. 2014; 63:128–140. Doi 10.1016/j.jmps.2013.09.015. [PubMed: 24563551]
36. Reimink MS, Kunzelman KS, Cochran RP. The effect of chordal replacement suture length on function and stresses in repaired mitral valves: a finite element study. J Heart Valve Dis. 1996; 5:365–375. [PubMed: 8858500]
37. Rim Y, Laing ST, Kee P, McPherson DD, Kim H. Evaluation of mitral valve dynamics. JACC Cardiovasc Imaging. 2013; 6:263–268. Doi 10.1016/j.jcmg.2012.10.017. [PubMed: 23489540]
38. Rim Y, McPherson DD, Chandran KB, Kim H. The effect of patient-specific annular motion on dynamic simulation of mitral valve function. J Biomech. 2013; 46:1104–1112. Doi 10.1016/j.jbiomech.2013.01.014. [PubMed: 23433464]
39. Savage DD, Garrison RJ, Devereux RB, Castelli WP, Anderson SJ, Levy D, McNamara PM, Stokes J 3rd, Kannel WB, Feinleib M. Mitral valve prolapse in the general population. 1. Epidemiologic features: the Framingham Study. Am Heart J. 1983; 106:571–576. [PubMed: 6881031]
40. Shah PM. Current concepts in mitral valve prolapse--diagnosis and management. J Cardiol. 2010; 56:125–133. Doi 10.1016/j.jjcc.2010.06.004. [PubMed: 20702064]
41. Sonne C, Sugeng L, Watanabe N, Weinert L, Saito K, Tsukiji M, Yoshida K, Takeuchi M, Mor-Avi V, Lang RM. Age and body surface area dependency of mitral valve and papillary apparatus parameters: assessment by real-time three-dimensional echocardiography. Eur J Echocardiogr. 2009; 10:287–294. Doi 10.1093/ejechocard/jen237. [PubMed: 18799478]
42. Stevanella M, Votta E, Redaelli A. Mitral valve finite element modeling: implications of tissues' nonlinear response and annular motion. J Biomech Eng. 2009; 131:121010. Doi 10.1115/1.4000107. [PubMed: 20524733]

43. Votta E, Maisano F, Bolling SF, Alfieri O, Montevecchi FM, Redaelli A. The Geoform disease-specific annuloplasty system: a finite element study. Ann Thorac Surg. 2007; 84:92–101. Doi 10.1016/j.athoracsur.2007.03.040. [PubMed: 17588392]

44. Wenk JF, Ratcliffe MB, Guccione JM. Finite element modeling of mitral leaflet tissue using a layered shell approximation. Med Biol Eng Comput. 2012; 50:1071–1079. Doi 10.1007/s11517-012-0952-2. [PubMed: 22971896]

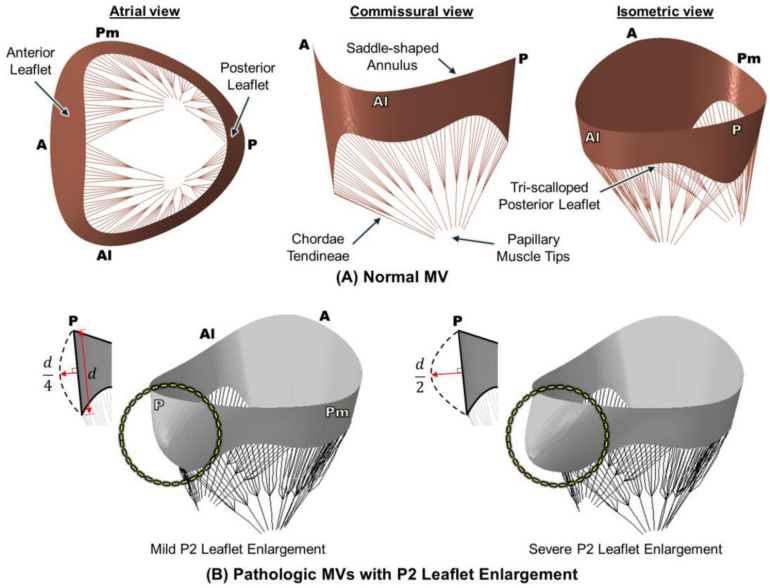

Figure 1.

(A) Parametric normal MV geometry model at end diastole (A – anterior, P – posterior, Al – anterolateral, Pm – posteromedial). (B) Pathologic MVs with mild and severe P2 leaflet enlargement.

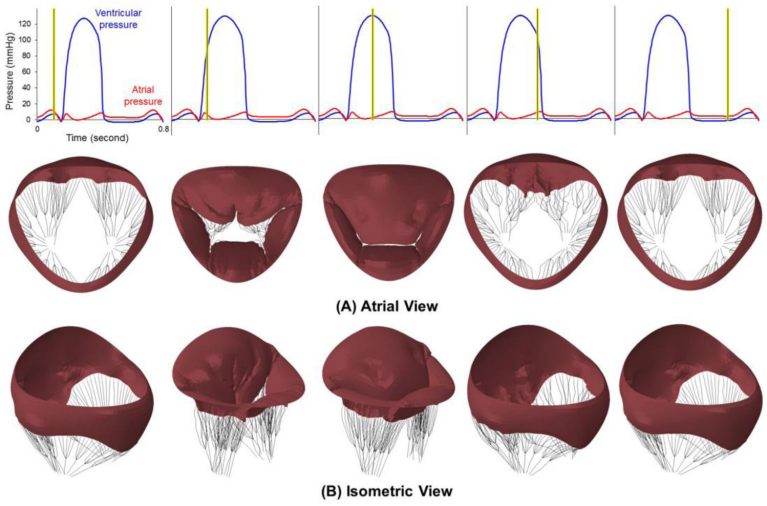

Figure 2.

Morphologic characteristics of the normal MV at five representative time points over the cardiac cycle computed from the dynamic FE simulation of MV function

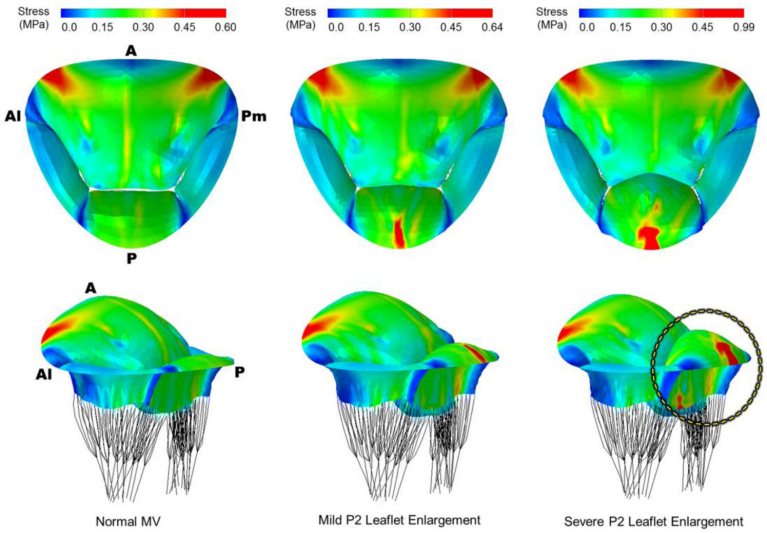

Figure 3.

Stress distributions across the mitral leaflets and annulus at peak systole following P2 leaflet enlargement.

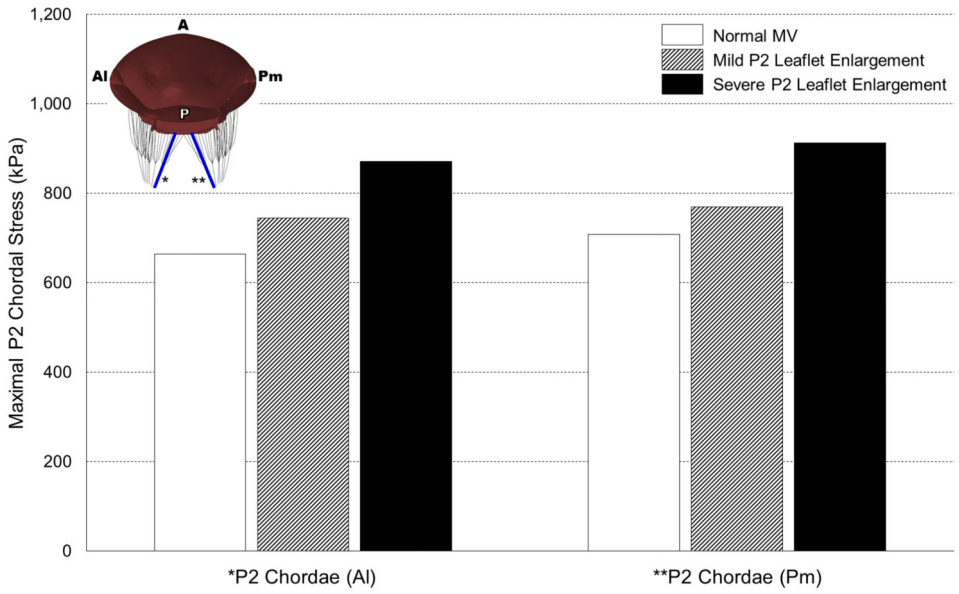

Figure 4.
Maximal posterior chordal stress values at peak systole following P2 leaflet enlargement.

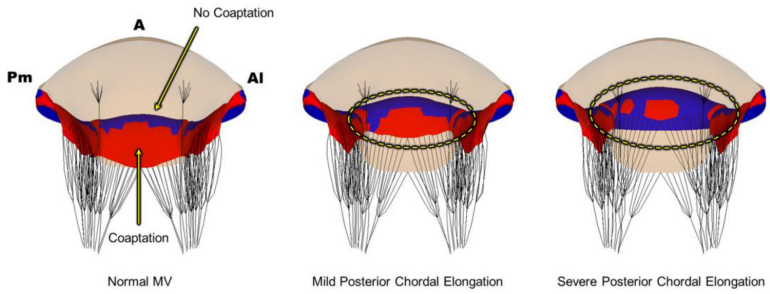

Figure 5.
Leaflet coaptation at peak systole in the normal MV and the MVs with posterior chordal elongation.

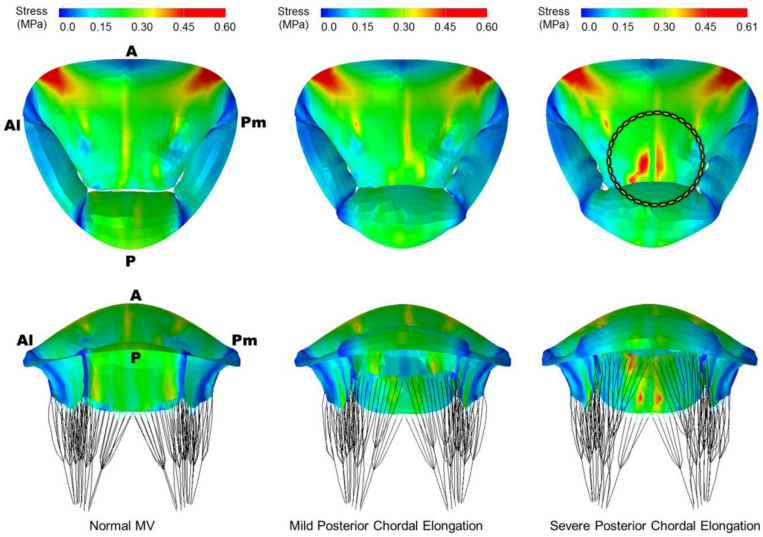

Figure 6.

Stress distributions across the mitral leaflets and annulus at peak systole following posterior chordal elongation.

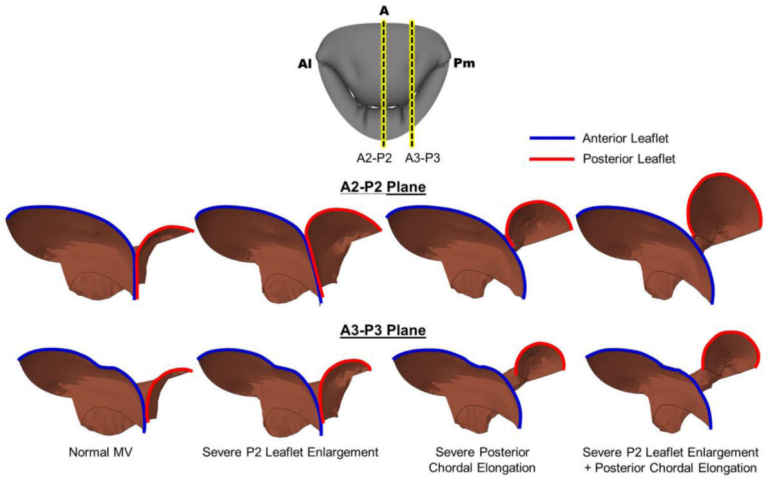

Figure 7.

Leaflet morphologies at peak systole in the normal MV and the pathologic MVs with severe P2 leaflet enlargement, severe posterior chordal elongation, and a combination of these two abnormalities.

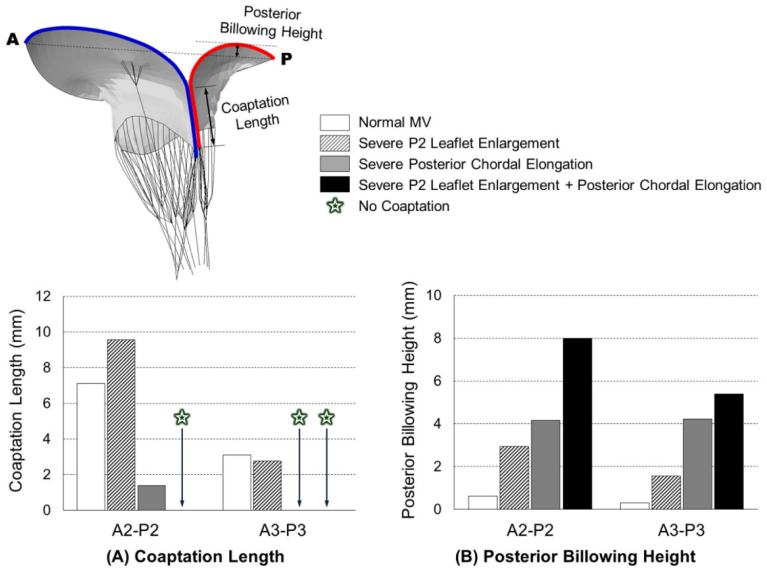

Figure 8.

Coaptation lengths and posterior billowing heights at peak systole in the MV models having normal pathophysiology, severe P2 leaflet enlargement, severe posterior chordal elongation, and a combination of these two abnormalities.